

Analytical Estimation of Reactive Power Capability of a Radial Distribution System

Stefan Stanković, *Student Member, IEEE* and Lennart Söder, *Senior Member, IEEE*

Abstract—The control of reactive power exchange between grids of different voltage levels has always been a concern for system operators. With production moving from the transmission to the distribution level, its importance increases. This paper proposes a novel approach to estimate reactive power capability of the grid as a whole. A linearized analytical model for an estimation of available reactive power exchange at the interface between two grids has been developed. The maximum estimation error for the scenarios we tested was only 2%. The model gives the relation between important grid parameters and the supported reactive power. The conclusions drawn from the model are confirmed on typical Swedish distribution network with scattered wind power and small industry consumers. Common scenarios in development of distribution grids are applied to show relevant parameters influence. One studied scenario is replacement of overhead lines with cables. It is shown that this particular change enhances the reactive power capability of the grid which is directly seen from the analytical analysis without running any optimal power flow. The analytical model proposed in this paper gives fundamental understanding of the reactive power capability of radial distribution grids.

Index Terms—distribution grid, reactive power capability, reactive power management, voltage control, wind power

I. INTRODUCTION

THERE is an increasing number of countries identifying importance of renewable, eco-friendly energy sources. This is confirmed by adopting law-based obligatory documents and directives [1], [2]. In order to meet the goals of these, decommissioning of large generation units situated in a transmission network and emergence of distributed generation (DG) in distribution grids has started and it is likely to continue in the future. The future development brings bigger penetration of DG and cables in the grid and consequently brings new problems to be solved. One of them is more common reversed active power flows. Another one that is a topic of this paper is control of reactive power flow at the point of common coupling (PCC) between the grids of different voltage levels.

Most of the control actions in power grids are driven by economic matters. In order to increase the profit, maximizing active power generation and reducing active power losses are used as the criteria. Therefore, most distribution system operators (DSO) have regulations from which DG is expected to operate at constant power factor equal to one, thus not providing nor consuming reactive power [3], [4]. But, the benefit of reactive power support from DG in distribution grids has been recognized by certain DSOs [4], [5]. Economic side of it comes in the light of emerging reactive power markets [6], [7]. Certain transmission system operators have already formed them [4], [8]. In these, DSOs can participate by providing reactive support to a transmission system. Euro-

pean Union legislation documents are following the trend by recommending the change of national grid codes [9].

There has been a lot of discussion about benefits of ancillary service provision and reactive power support from DG. The discussions are furthermore expanded to its contribution to reactive power control or management at the PCC [10]–[24]. The ability of the distribution grid to control reactive power at the PCC is commonly denoted in the mentioned papers as the reactive capability of the grid. It defines minimum and maximum boundary of reactive power that can be supported at the PCC depending on active power transfer at the PCC. The same term will be used throughout this paper. Some of the papers [10]–[15] are identifying reactive capability of the grid for certain case studies and time frames. Others [15]–[24] are discussing different control strategies for reactive power management at the PCC.

However, none of these papers is trying to find analytical relation between parameters of the radial grid and its reactive power capability. This paper provides a linearized analytical model that fills in the gap. The model has been developed and confirmed on representative case studies. The case studies illustrate typical scenarios in development of distribution systems. They include exchange of overhead lines in the grid with cables or different dispositions of DG and small industry loads.

Nowadays, increased number of cables in distribution grids creates overvoltage problems [25], [26]. Certain DSOs decided to install inductors at substations to keep the voltage down, compensate and avoid injection of excessive reactive power into the overlaying grid. Although it solves temporarily the overvoltage problems, the analytical model shows that it degrades grid reactive power capability. Without compromising the reactive power capability, the problems can be solved using DG for compensation of reactive power. This way, the grid keeps ability to respond to the future challenges.

The benefit of analytical modeling is that it gives fundamental understanding of the problem. By use of the analytical model of reactive power capability, without sensitivity analysis, conclusions about influence from different grid parameters on reactive capability can be drawn. Fast estimation of available reactive power at the PCC can also be done without running computationally demanding optimal power flows (OPF). The maximum estimation error for the scenarios we tested was only 2% of the range in which reactive power can be controlled at the PCC.

Knowledge of the distribution system capability to provide reactive power is of great technical as well as economical importance [24], [27]. Conclusions of this paper provide answers where to make changes and how to reinforce the grid

for the future and present needs of providing reactive support.

II. PROBLEM FORMULATION

The system that will be analyzed is a typical radial distribution network with randomly located wind power plants and loads. Objective of the analysis is to find out possibilities and limitations of distribution grids to support transmission grids with reactive power. This objective is commonly known as reactive power capability of the distribution grid. Mathematically, the problem can be described as an optimization task:

$$\begin{aligned}
 \text{obj.} \quad & \min(Q_{PCC}), \quad \max(Q_{PCC}) \\
 \text{s.t.} \quad & \sum P_{inj_i} = 0 \\
 & \sum Q_{inj_i} = 0 \\
 & U_{min_i} < U_i < U_{max_i}, \\
 & Q_{min_j} < Q_j < Q_{max_j}, \\
 & \forall i \in Bus, \forall j \in Gen
 \end{aligned} \tag{1}$$

where the equality constraints comprise the power balance at each bus of the system. Injected active and reactive power at bus i are denoted with P_{inj_i} and Q_{inj_i} . The reactive power exchange at the PCC $Q_{PCC} = f_Q(x, par)$ is a multi-variable, nonlinear function of system states x and parameters par . When it comes to the reactive power support, parameters of special interest include:

- length of the line sections
- R/X ratio of the line sections
- location of DG (e.g. wind power)
- location of loads

Beside parameters, state variables of the system have to be observed too. They can be divided into two groups: controllable and non-controllable.

The first group consists of the voltages U_i and/or reactive powers Q_j of generating units in the grid contained in the set of generator buses Gen . The set Gen is a subset of set of all the buses in the system Bus . Most important non-controllable variables for the purpose of the analysis in this paper are active powers on the lines of the grid. Their influence on the reactive support has to be analyzed.

Inequality constraints define physical limits of the system:

- voltage limits on the buses
- reactive power limits of the generating units

Reactive power outputs of generating units as control variables are bounded by reactive power limits. These limits are defined by capability curves of the generating units and associated power electronics devices [28]–[30]. In the most basic form, these limits can be approximated with (2).

$$Q_{lim} = \pm \sqrt{S_n^2 - P^2} \tag{2}$$

where S_n is nominal power of the generator, P -current active power production and Q_{lim} -current reactive power limits. The approximation (2) is used by [18], [23]. Since this paper is focusing more on the grid perspective, (2) will be used in this paper without compromising the final results.

III. MATHEMATICAL ANALYSIS

Importance of analytical description of the problem primarily comes from the need to draw general conclusions about the grids and their parameters that are important when it comes to reactive power provision from a distribution grid to a transmission grid. The final objective is to find relation $Q_{PCC} = f_Q(x, par)$ and separate influence from the following six factors:

- 1) voltage rise/drop over a section,
- 2) active power exchange at the PCC,
- 3) disposition of injected reactive power,
- 4) disposition of injected active power,
- 5) R/X ratios of lines
- 6) active and reactive power losses in the grid.

In order to do it, the distribution grid is divided into sections. One section represents path between two buses in a grid such that going from one bus (B_{k1}) towards another one (B_{k2}), descend down the tree hierarchy of a radial distribution grid is respected (Fig. 1).

For the purpose of our analysis, we used π model of lines for positive sequence as in [12], [14]–[17], [20], [22]. Parameters of the line, active and reactive power flows change along a section. In order to account for these changes, the section is represented as a sum of small subsections with constant parameters and power flows (Fig. 2). Each subsection i connects nodes with indexes $i - 1$ and i and has the same electrical length meaning that reactances of the subsections are the same $X_i = \Delta X, i = 1..N$. Related active and reactive power flows through the subsection i measured at node $i - 1$ are respectively P_i and Q_i . At each node i there is an active $P_{(i)inj}$ and a reactive power injection $Q_{(i)inj}$. Each subsection i has constant resistance R_i and reactance $X_i = \Delta X$. Capacitance of the subsections are included through reactive power injections on neighboring nodes.

For each subsection, voltage drop equation could be written:

$$\underline{U}_i = \underline{U}_{i-1} + \frac{P_i R_i + Q_i X_i}{\underline{U}_{i-1}^*} + j \frac{P_i X_i - Q_i R_i}{\underline{U}_{i-1}^*} \tag{3}$$

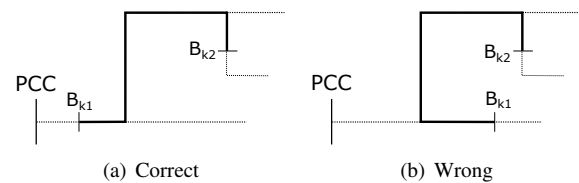


Fig. 1. Proper way of defining a section

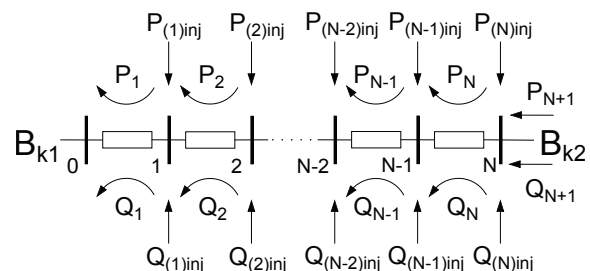


Fig. 2. Line section of the grid divided into subsections

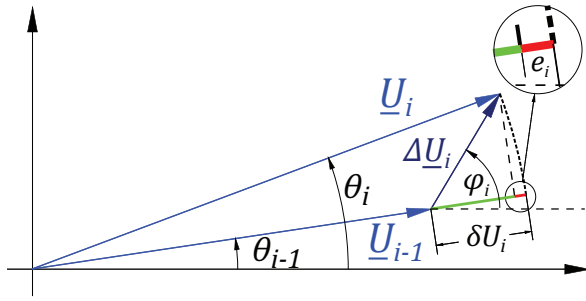


Fig. 3. Voltage drop equation in complex plane

where \underline{U}_i is a complex voltage at node $i, i = 1..N$ and j is imaginary unit. Representation of all complex voltages as phasors in complex plane is shown on Fig. 3. Here, the complex voltage drop is introduced as $\Delta \underline{U}_i = \Delta U_i \angle \varphi_i$. By multiplying both sides of (3) with \underline{U}_{i-1}^* and rewriting it according to Fig. 3, following equation is formed:

$$\begin{aligned} U_{i-1} \Delta U_i (\cos(\varphi_i - \theta_{i-1}) + j \sin(\varphi_i - \theta_{i-1})) = \\ = P_i R_i + Q_i X_i + j(P_i X_i - Q_i R_i) \end{aligned} \quad (4)$$

From phasor diagram on Fig. 3 it can be seen that absolute voltage drop $\delta U_i = |\underline{U}_i| - |\underline{U}_{i-1}|$ has similar value as the projection of complex voltage drop phasor $\Delta \underline{U}_i$ on phasor \underline{U}_{i-1} :

$$\delta U_i = |\underline{U}_i| - |\underline{U}_{i-1}| = \text{proj}_{U_{i-1}}(\Delta \underline{U}_i) + \epsilon_{U_i} \quad (5)$$

where the projection $\text{proj}_{U_{i-1}}(\Delta \underline{U}_i) = \Delta U_i \cos(\varphi_i - \theta_{i-1})$ is drawn with the green line and associated approximation error ϵ_{U_i} is drawn with the red line on Fig. 3. Taking real parts of (4) and writing it for all the subsections $i = 1..N$ while taking into account (5), summation of the formed system of equations will be:

$$\sum_{i=1}^N (U_{i-1} \delta U_i) - \epsilon_Q \Delta X = \sum_{i=1}^N (P_i R_i + Q_i X_i) \quad (6)$$

where $\epsilon_Q = \frac{1}{\Delta X} \sum_{i=1}^N U_{i-1} \epsilon_{U_i}$ accounts for the approximation error.

Geometric position of phasor U_i tip with varying Q_i is shown with red, dotted line on Fig. 4 where $\tan \xi_i = R_i/X_i$. It can be seen that δU_i and $\text{proj}_{U_{i-1}}(\Delta \underline{U}_i)$ (green line) increase with increasing Q_i and both decrease with decrease of Q_i . The

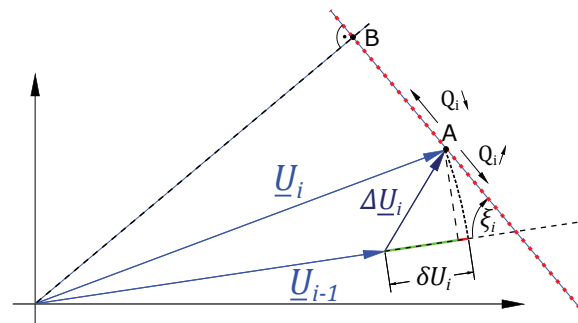


Fig. 4. Geometric position of U_i with varying Q_i

trend is not true only for the points that are further to the left from the point B (Fig. 4) since the decrease of Q_i results in the increase of U_i . These points are not reached in practice because they violate voltage and current (thermal) constraints of the grid. For other points, (6) can be used for comparative analysis of different scenarios.

Ratio R_i/X_i might vary along the section. Since reactance is the same for each subsection this means that resistance of different subsections might not be equal. In order to account for these variations, coefficient r_i is introduced:

$$r_i = \frac{R_i}{\Delta R} \quad (7)$$

Parameter ΔR can be chosen arbitrary. If it is defined as $\Delta R = R_1$ then r_i describes the change of R_i/X_i ratio of the line relative to ratio at the beginning of the section. If $\Delta R = \Delta X$ then r_i represents exact R_i/X_i ratio at the position i . Dividing both sides of (6) with ΔX , having in mind (7) it becomes:

$$\frac{\bar{U}}{\Delta X} \sum_{i=1}^N \Delta U_i - \epsilon_Q = \frac{\Delta R}{\Delta X} \sum_{i=1}^N r_i P_i + \sum_{i=1}^N Q_i \quad (8)$$

where \bar{U} is average voltage of the section.

In order to get information about dependency of generation and load disposition along the section it would be convenient to express active and reactive power flows P_i, Q_i in terms of active and reactive power injections $P_{(i)inj}, Q_{(i)inj}$. This relation can be found if first Kirchoff law in a form of complex powers is written for each node i . If real and imaginary parts are separated, it becomes:

$$P_i + \Delta P_i = P_{(i)inj} + P_{i+1} \quad (9a)$$

$$Q_i + \Delta Q_i = Q_{(i)inj} + Q_{i+1} \quad (9b)$$

where ΔP_i and ΔQ_i are active and reactive power losses on the subsection i . By writing (9a,9b) for every node i and expressing P_{i+1} and Q_{i+1} , two sets of equations are assembled:

$$\begin{aligned} P_2 &= P_1 - P_{(1)inj} + \Delta P_1 \\ P_3 &= P_2 - P_{(2)inj} + \Delta P_2 \\ &\vdots \end{aligned} \quad (10a)$$

$$\begin{aligned} P_{N-1} &= P_{N-2} - P_{(N-2)inj} + \Delta P_{N-2} \\ P_N &= P_{N-1} - P_{(N-1)inj} + \Delta P_{N-1} \\ &\dots\dots\dots \\ Q_2 &= Q_1 - Q_{(1)inj} + \Delta Q_1 \\ Q_3 &= Q_2 - Q_{(2)inj} + \Delta Q_2 \\ &\vdots \\ Q_{N-1} &= Q_{N-2} - Q_{(N-2)inj} + \Delta Q_{N-2} \\ Q_N &= Q_{N-1} - Q_{(N-1)inj} + \Delta Q_{N-1} \end{aligned} \quad (10b)$$

P_2 in second equation can be expressed from first equation of (10a). If P_3 in third equation is then expressed from newly assembled form of second equation and the process is repeated

for all the equations in (10a), new set of equations is formed (11a). It explicitly gives relation between active powers on the subsections of the line and active powers injected into nodes $P_{(i)inj}$ including the one supplied to the transmission grid P_1 . The same process is repeated with (10b) for obtaining (11b). It includes much more important quantity, reactive power supplied to the transmission grid Q_1 .

$$\begin{aligned} P_2 &= P_1 - P_{(1)inj} + \Delta P_1 \\ P_3 &= P_1 - \sum_{i=1}^2 P_{(i)inj} + \sum_{i=1}^2 \Delta P_i \\ &\vdots \end{aligned} \quad (11a)$$

$$\begin{aligned} P_{N-1} &= P_1 - \sum_{i=1}^{N-2} P_{(i)inj} + \sum_{i=1}^{N-2} \Delta P_i \\ P_N &= P_1 - \sum_{i=1}^{N-1} P_{(i)inj} + \sum_{i=1}^{N-1} \Delta P_i \\ &\dots\dots\dots \\ Q_2 &= Q_1 - Q_{(1)inj} + \Delta Q_1 \\ Q_3 &= Q_1 - \sum_{i=1}^2 Q_{(i)inj} + \sum_{i=1}^2 \Delta Q_i \\ &\vdots \\ Q_{N-1} &= Q_1 - \sum_{i=1}^{N-2} Q_{(i)inj} + \sum_{i=1}^{N-2} \Delta Q_i \\ Q_N &= Q_1 - \sum_{i=1}^{N-1} Q_{(i)inj} + \sum_{i=1}^{N-1} \Delta Q_i \end{aligned} \quad (11b)$$

By substituting active and reactive powers (P_i , Q_i) in (8) with powers from (11a, 11b) following equation is formed:

$$\begin{aligned} \frac{\bar{U}}{\Delta X} \Delta U &= \frac{\Delta R}{\Delta X} (P_1 \sum_{i=1}^N r_i - \sum_{i=1}^{N-1} (P_{(i)inj} \sum_{j=i+1}^N r_j) \\ &+ NQ_1 - \sum_{i=1}^{N-1} (N-i)Q_{(i)inj} + \epsilon_Q \\ &+ \frac{\Delta R}{\Delta X} \sum_{i=1}^{N-1} (\Delta P_i \sum_{j=i+1}^N r_j) + \sum_{i=1}^{N-1} (N-i)\Delta Q_i \end{aligned} \quad (12)$$

where ΔU is total voltage change along the analyzed section.

From (12), supported reactive power Q_1 can be expressed:

$$\begin{aligned} Q_1 &= \bar{U} \frac{\Delta U}{N\Delta X} + \sum_{i=1}^{N-1} \frac{(N-i)}{N} Q_{(i)inj} - \epsilon_Q \\ &- \frac{\Delta R}{\Delta X} (P_1 \frac{1}{N} \sum_{i=1}^N r_i - \sum_{i=1}^{N-1} (P_{(i)inj} \frac{1}{N} \sum_{j=i+1}^N r_j) \\ &- \frac{\Delta R}{\Delta X} \sum_{i=1}^{N-1} (\Delta P_i \frac{1}{N} \sum_{j=i+1}^N r_j) - \sum_{i=1}^{N-1} \frac{(N-i)}{N} \Delta Q_i \end{aligned} \quad (13)$$

Equation (13) defines reactive power at the beginning of the section Q_1 as a function of the six factors listed at the

beginning of the paper section III. The final goal is to find relation between them and the reactive power capability of the whole grid (Q_{PCC}).

A. Application on a radial grid

Equation (13) gives the information only for the one section of the grid. The same equation can be used to derive conclusions about the whole radial grid.

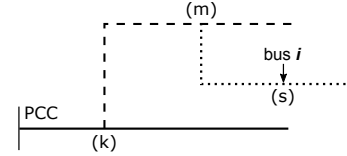


Fig. 5. The part of a radial distribution grid

Fig. 5 illustrates part of the radial distribution grid. The grid is divided into sections such that each section represents one branch of the grid. The main branch (full line) is the parent section of branch 1 (dashed line). Branch 1 is the parent section of branch 2 (dotted line). Branch 1 is connected at position k on the main branch while branch 2 is connected at position m on the branch 1. For each of the branches, equation (13) can be written. Writing it for the main branch and branch 1, (14a) and (14b) are obtained:

$$\begin{aligned} Q_{PCC} &= \bar{U} \frac{\Delta U}{N\Delta X} + \sum_{i=1}^{N-1} \frac{(N-i)}{N} Q_{(i)inj} - \epsilon_Q \\ &- \frac{\Delta R}{\Delta X} (P_{PCC} \frac{1}{N} \sum_{i=1}^N r_i - \sum_{i=1}^{N-1} (P_{(i)inj} \frac{1}{N} \sum_{j=i+1}^N r_j) \\ &- \frac{\Delta R}{\Delta X} \sum_{i=1}^{N-1} (\Delta P_i \frac{1}{N} \sum_{j=i+1}^N r_j) - \sum_{i=1}^{N-1} \frac{(N-i)}{N} \Delta Q_i \end{aligned} \quad (14a)$$

$$\begin{aligned} Q_{(k)inj} &= \bar{U}_I \frac{\Delta U_I}{N_I \Delta X} + \sum_{i=1}^{N_I-1} \frac{(N_I-i)}{N_I} Q_{I(i)inj} - \epsilon_{Q_I} \\ &- \frac{\Delta R}{\Delta X} (P_{(k)inj} \frac{1}{N_I} \sum_{i=1}^{N_I} r_{Ii} - \sum_{i=1}^{N_I-1} (P_{I(i)inj} \frac{1}{N_I} \sum_{j=i+1}^{N_I} r_{Ij}) \\ &- \frac{\Delta R}{\Delta X} \sum_{i=1}^{N_I-1} (\Delta P_{Ii} \frac{1}{N_I} \sum_{j=i+1}^{N_I} r_{Ij}) - \sum_{i=1}^{N_I-1} \frac{(N_I-i)}{N_I} \Delta Q_{Ii} \end{aligned} \quad (14b)$$

where index I in (14b) denotes that quantities belong to the branch 1. $Q_{(k)inj}$ obtained from (14b) can be used in (14a). If (14b) is written for each child section of the grid and the equations are used in their parents' section equations, (15) is formed.

$$\begin{aligned} Q_{PCC} &= \sum_{i \in B} \eta_i \bar{U}_i \frac{\Delta U_i}{N_i \Delta X} + \sum_{i \in Bus} \eta_i Q_{(i)inj} - \epsilon_{Q_{PCC}} \\ &- \frac{\Delta R}{\Delta X} \sum_{i \in Bus} \eta_i (\bar{r}_{ch(i)} - \bar{r}_{p(i)}) P_{(i)inj} \\ &- \frac{\Delta R}{\Delta X} \sum_{i \in Bus} \bar{r}_{p(i)} \eta_i \Delta P_i - \sum_{i \in Bus} \eta_i \Delta Q_i \end{aligned} \quad (15)$$

Here Bus represents the set of all buses while B is the set of all branches in the grid. In the case of Fig. 5, $B = \{\{\}, I, II\}$ where the main branch is denoted with an empty element. Relative electrical proximity of the node i in the system is described with coefficient η_i . Its value can be found as follows:

$$\eta_i = \prod_{j \in \gamma_i} \frac{N_j - c_j}{N_j} \quad (16)$$

where γ_i is a subset of B containing all the branches on the path between the PCC and the bus i . Position on the branch j at which it coincides with the next branch on the path is denoted with c_j . In the case that branch j is the last branch on the path, c_j is the position of the bus i on the branch j . As an example, relative electrical proximity of bus i on Fig. 5 is:

$$\eta_i = \frac{N - k}{N} \frac{N_I - m}{N_I} \frac{N_{II} - s}{N_{II}} \quad (17)$$

Active power injections ($P_{(i)inj}$) in (15) are generalized including injections of active power from the child sections to the parent sections. Consecutively, parameters $\bar{r}_{ch(i)}$ and $\bar{r}_{p(i)}$ are introduced. If $P_{(i)inj}$ comes from the child section, $\bar{r}_{ch(i)}$ is defined as the average value of r_i described by (7) over that section. Otherwise, $\bar{r}_{ch(i)} = 0$. Parameter $\bar{r}_{p(i)}$ averages r_i over residue of the parent section (path from the position of bus i on the parent section until the end of it).

Total approximation error $\epsilon_{Q_{PCC}}$ is given by (18).

$$\epsilon_{Q_{PCC}} = \sum_{i \in B} \eta_i \epsilon_{Q_i} \quad (18)$$

By setting limits on the input variables on the right side of (15), voltage limits, line current limits and reactive power limits of DG can be accounted. For example, current limit on the line connecting buses 6 and 7 should be accounted by limiting the value of active power losses on that line ΔP_7 . ΔP_7 is part of the sum at the last row of (15).

B. Conclusions from the analytical model

The terms in (15) describe influences of relevant factors from the beginning of paper section III on inductive ($Q_{min(PCC)} = \min(Q_{PCC})$) and capacitive ($Q_{max(PCC)} = \max(Q_{PCC})$) reactive power capability of the grid. These terms are from here on distinguished as:

- U term: First term in the first row corresponding to the voltage profile of the grid.
- Q term: Second term in the first row corresponding to distribution of reactive power injections.
- P term: Expression in the second row corresponding to total active power exchange at the PCC and its distribution in the grid.
- loss term: Expression in the last row describing distribution of power losses in the grid.
- error term: Third term in the first row that accounts for error made by approximation in (5).

From them, conclusions about the influences are drawn:

1) Voltage rise/drop

U term shows that reactive power supported to a transmission grid is proportional to a mean rate of change of voltage according to electrical distance from the PCC ($\frac{\Delta U_i}{N_i \Delta X}$). This means that in order to maximize/minimize reactive power Q_{PCC} , upper/lower limit of the voltage should be reached as close electrically as possible.

2) Active power exchange at the PCC

If active power is exported to the PCC, consecutively $Q_{max(PCC)}$ will decrease and $Q_{min(PCC)}$ will increase. On the other way, if active power is imported from the PCC, $Q_{max(PCC)}$ will increase and $Q_{min(PCC)}$ will decrease. This can be concluded from the element $i = PCC$ of the sum in P term. For it $P_{(i)inj} = P_{PCC}$, and $\eta_i = 1$. Here $\bar{r}_{ch(i)}$ represents average value of r_i over the first section. Parameter $\bar{r}_{p(i)} = 0$ since the section starts from the PCC and therefore does not have a parent section. Now it can be seen that $Q_{PCC} \propto -P_{PCC}$ leading to the obtained conclusions.

3) Disposition of injected reactive power

In order to have better controllability of Q_{PCC} , Q term shows that injected reactive power should be kept as close as possible to the PCC. This is the case since the sum of Q term is weighted with electrical proximity η_i (17). This furthermore means that keeping generation as close as possible to the PCC and reactive loads further from it will increase $Q_{max(PCC)}$ and decrease $Q_{min(PCC)}$. If reactive power generation is further from the PCC and reactive power consumption is closer, $Q_{max(PCC)}$ will decrease and $Q_{min(PCC)}$ will increase.

4) Disposition of injected active power

For the fixed export of active power P_{PCC} it is interesting to see how the distribution of this power in the grid affects available reactive power Q_{PCC} . This can be done by observing the P term. For the active power injections that do not come from child section, $\bar{r}_{ch(i)} = 0$ and $\bar{r}_{p(i)} > 0$. This means that active power injections $P_{(i)inj}$ in the grid, having in mind fixed active power export P_{PCC} , are directly proportional to Q_{PCC} with proportionality constant $\eta_i \bar{r}_{p(i)}$. This leads to the conclusion that keeping the active power generation closer and loads further from the PCC will increase $Q_{max(PCC)}$ and decrease $Q_{min(PCC)}$. The effects are opposite if the loads are closer and generation is further away from the PCC.

5) R/X ratios of lines

Higher R/X ratios increase the influence of active powers on Q_{PCC} as seen from the P term. An interesting observation can be made regarding the injected power $P_{(ch(i))inj}$ from the child to the parent section. If $\bar{r}_{ch(i)} > \bar{r}_{p(i)}$, $Q_{PCC} \propto -P_{(ch(i))inj}$. The voltage drop/rise created by $P_{(ch(i))inj}$ will favor the reactive power flow in the opposite direction from $P_{(ch(i))inj}$ on the child section. If $\bar{r}_{ch(i)} < \bar{r}_{p(i)}$ then $Q_{PCC} \propto P_{(ch(i))inj}$. $P_{(ch(i))inj}$ will have positive effect on Q_{PCC} since it would relief residue of the parent section, more prone to voltage rise/drop, from active power flows. The effect is pronounced for the cases where a weak line (usually with higher R/X ratio) is connected with a strong line (cable feeder). The $P_{(ch(i))inj}$ will have much smaller influence on voltage profile on the

strong line than on the weak line. For the cases where $\bar{r}_{ch(i)} \sim \bar{r}_{p(i)}$, the effect is negligible.

6) *Active and reactive power losses*

Loss term shows that both active and reactive power losses in the system will decrease $Q_{max(PCC)}$ but increase $Q_{min(PCC)}$. If the losses are closer to the PCC, the effect will be more pronounced since the elements in the loss term sum are also weighted with electrical proximity η_i .

IV. NUMERICAL CONFIRMATION OF ANALYTICAL CONCLUSIONS

In order to confirm obtained analytical results from section III, numerical confirmation will be done in this section. The radial distribution grid shown on Fig. 6 is used as a test system. It represents typical 10kV radial distribution network common in Swedish rural areas.

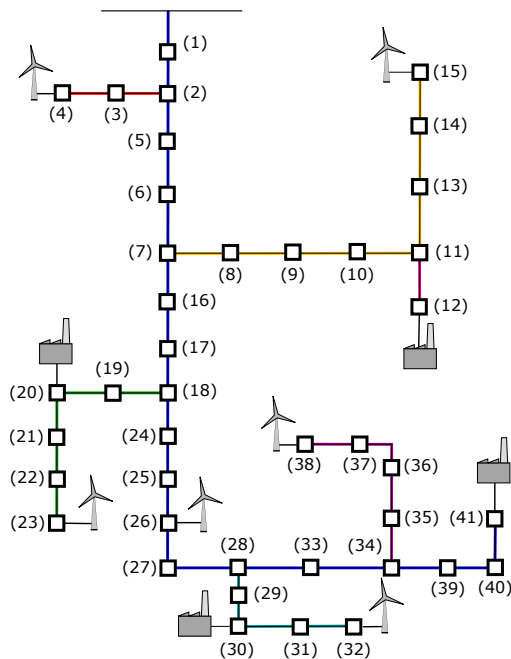


Fig. 6. Typical rural Swedish distribution grid with DG

The grid consist mainly of overhead lines with R/X ratios ranging from $R/X = 1$ to $R/X = 2.4$. Besides distributed residential consumption, the grid hosts also small industry consumers (0.5MW to 1.5MW) with power factor around 0.98. DFIG wind turbines in the range of 1MW to 2MW with reactive power capabilities described by (2) have been integrated in the grid.

Voltage limits are assumed to be $U_{lim} = \pm 3\%U_n$ where $U_n = 10kV$ is the rated voltage of the grid. Bus 1 is assumed to be the low voltage side of the transformer equipped with the on load tap changer. It is assumed that voltage at the bus 1 can be varied in the range of the operating limits of the grid. Using MATPOWER's OPF algorithm [31], (1) is solved to find a reactive capability of the grid. Buses with connected DG are modeled as PU buses while others are set to be PQ buses. As controlled inputs to the OPF algorithm, voltage amplitudes of the PU buses and voltage at the bus 1 (slack bus) are used.

In order to test conclusions from section III-B, different scenarios common in practice are used for comparative analysis. Scenarios illustrate the change of certain parameters of interest from (13) and (15) while keeping other parameters constant.

To analyze influence of different loading scenarios of the grid on reactive power provision at the PCC, two cases are assembled:

- 1) distributed generation at 80% of maximum, consumption at 70% of maximum
- 2) distributed generation not producing (possible reactive support), consumption at maximum

First case represents the scenario with high active power export towards a transmission grid. The second one represents the scenario with high active power import from a transmission grid.

It is very common that with development of distribution grids, parts of overhead lines are being replaced with cables [32]. The influence on reactive power provision at the PCC is assessed by exchanging the overhead lines connecting buses 1, 2, 5, 6, 7, 16, 17 and 18 with cables. It is assumed that the length of the lines stays the same. The reactances of the cables are smaller than those of the overhead lines which will result in decreased electrical distances. Since intersections of the lines stays the same, the resistance stays more or less the same. Consecutively, R/X ratios are increased now ranging from $R/X = 1.5$ to $R/X = 3.5$ on these sections.

The third change is related to disposition of consumption and DG in the grid. As a difference to the original disposition, locations of certain wind turbines and industry consumers are exchanged. The wind turbine at bus 15 is exchanged with consumer at bus 12. The same is done with the wind turbine at bus 23 and the consumer at bus 20.

The numerical results for all the described scenarios are shown in the Table I for disposition 1 and Table II for disposition 2. The voltage profiles of the cases with highest inductive and capacitive reactive power at the PCC are shown on Fig. 7 and Fig. 8.

A. Results

The conclusions derived in III-B are confirmed by comparing different scenarios applied to the grid. The influence of certain parameters on the grid's overall reactive power capability is assessed by comparing numerical values from Table I and Table II as well as voltage profiles on Fig. 7 and Fig. 8.

1) *Voltage rise/drop*

In order to set the utmost values of reactive power at the PCC, the OPF algorithm tends to create the biggest voltage rise/drop at the shortest electrical distance as possible. This fact is observed from the Fig. 7 and Fig. 8. The same conclusion has been anticipated by U term in (15).

2) *Active power exchange at the PCC*

An intuitive prediction made by P term in (15) has been confirmed by numerical results in Table I and Table II. The values of $Q_{min(PCC)}$ and $Q_{max(PCC)}$ show big dependence on active power exchange $P_{PCC}(Q_{PCC})$ at the PCC. Higher export of active power allows bigger

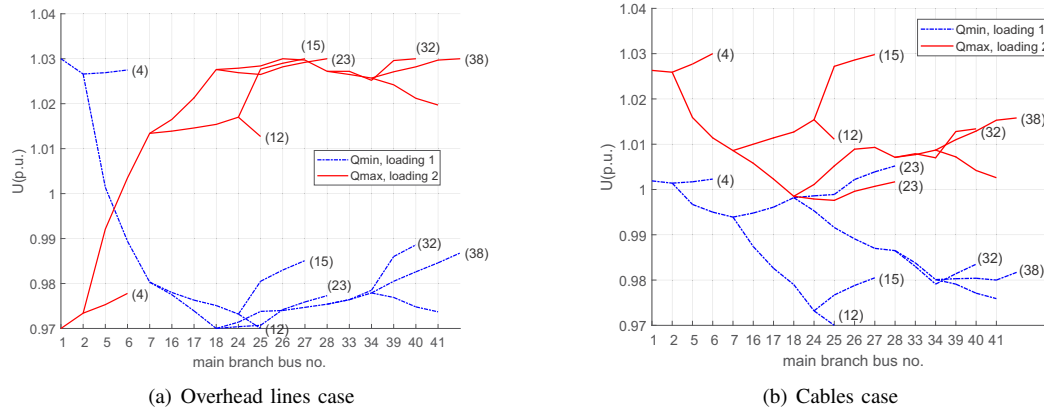


Fig. 7. Voltage profiles of the system for the disposition 1

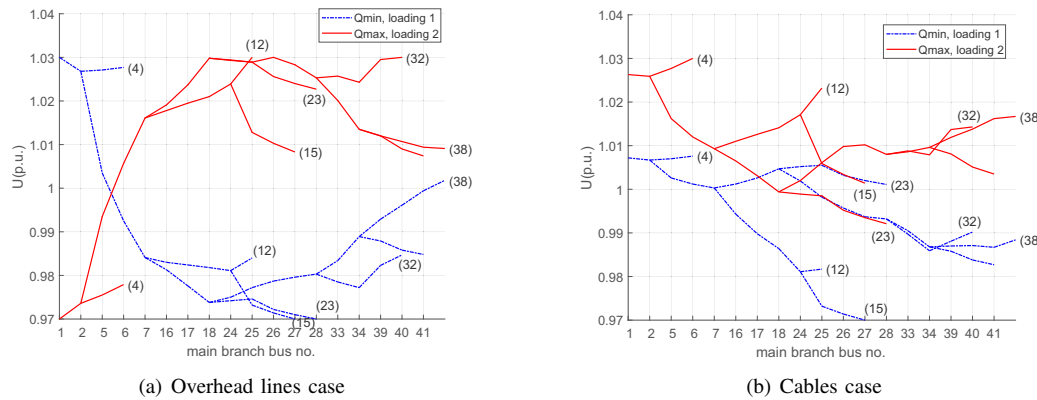


Fig. 8. Voltage profiles of the system for the disposition 2

import of reactive power. Higher import of active power allows bigger export of reactive power.

3.4) Production and consumption disposition

P term in (15) also predicts the influence of active power distribution on overall reactive power capability of the

grid. By comparing numerical values from Table I for disposition 1 and Table II for disposition 2 the predictions can be confirmed. The row corresponding to $Q_{max}(PCC)$ has smaller numerical values for disposition 1 than for disposition 2. This means that if the active power loads are closer to the PCC, $Q_{max}(PCC)$ will be smaller and vice versa. In order to increase $Q_{max}(PCC)$ active power generation should be as close as possible to the PCC. The opposite effect can be observed for $Q_{min}(PCC)$ by comparing values in the row corresponding to $Q_{min}(PCC)$ for both dispositions. The negative values in Table I are bigger than the ones in Table II. The inductive reactive power capability of the grid is therefore better for the case when the active power loads are closer to the PCC and generation is further away.

5) R/X ratios of lines

Exchange of overhead lines with cables in the grid has as a consequence increased R/X ratios of the lines and decreased electrical distances as a consequence of decreased reactances. This change has pronounced influence on reactive capability of the grid. Both inductive $Q_{min}(PCC)$ and capacitive $Q_{max}(PCC)$ capability are increased as can be seen from Table I and Table II comparing columns with values for overhead lines with the ones for cables case. The voltage profiles for overhead lines case are shown on Fig. 7(a) and Fig. 8(a). It can be seen that for both dispositions,

TABLE I

REACTIVE POWER PROVISION OF THE SYSTEM AT THE PCC FOR THE DISPOSITION 1

Provision at the PCC	overhead lines		cables	
	loading 1	loading 2	loading 1	loading 2
$Q_{min}(PCC)[p.u]$	-7.5686	-1.7508	-10.3446	-0.3132
$Q_{max}(PCC)[p.u]$	1.4577	8.2779	1.7111	11.1780
$P_{PCC}(Q_{min})[p.u]$	4.5555	-5.4932	3.8919	-5.4955
$P_{PCC}(Q_{max})[p.u]$	4.9725	-6.2104	4.9571	-6.8120

TABLE II

REACTIVE POWER PROVISION OF THE SYSTEM AT THE PCC FOR THE DISPOSITION 2

Provision at the PCC	overhead lines		cables	
	loading 1	loading 2	loading 1	loading 2
$Q_{min}(PCC)[p.u]$	-7.3231	-1.4464	-10.2999	0.5749
$Q_{max}(PCC)[p.u]$	1.9492	8.4410	2.7886	11.2076
$P_{PCC}(Q_{min})[p.u]$	4.6279	-5.4688	3.9978	-5.5527
$P_{PCC}(Q_{max})[p.u]$	4.9604	-6.1854	4.9612	-6.7345

voltage boundaries of the grid are the main limiting factor for provision of reactive power at the PCC. In the cables case, reactive power boundaries of the wind turbines are reached before voltage limits of the grid (Fig. 7(b), Fig. 8(b)). This means that the effect of exchanging overhead lines with cables would be even more pronounced if the reactive power boundaries of DG are bigger. The effect of R/X ratios on the reactive capability has been predicted as a part of P term and U term in (15). The numerical results confirm these predictions. With higher values of R/X ratios, active power flows create bigger voltage drops than reactive power flows. It consequently means that reactive power can be transported to bigger distances than active power.

6) Active and reactive power losses

The power losses should have negative influence on $Q_{max}(PCC)$ and positive influence on $Q_{min}(PCC)$ according to the loss term in (15). Although this influence is not highly pronounced, it can be observed on Fig. 8(b). In the case of maximizing reactive power export at the PCC, the OPF algorithm tries to maximize average voltage in the grid and decrease the power losses. If objective is to maximize reactive power import, the OPF minimizes average voltage to increase the power losses.

V. NUMERICAL ESTIMATION USING ANALYTICAL MODEL

Previous section confirmed qualitative conclusions derived from (15). In this section, (15) is used to get quantitative results and assess total approximation error $\epsilon_{Q_{PCC}}$. The assessment is done on two test grids:

- A) Swedish rural 10kV distribution grid (Fig. 6)
- B) IEEE 69 bus distribution grid (Fig. 9)

Before using (15), grids are divided into sections drawn with different colors as shown on Fig. 6 and Fig. 9. While doing so, the rule explained on Fig. 1 is respected. For both grids, maximum value of the total relative approximation error $\delta_{Q_{PCC}}$ defined by (19) is calculated for all loading scenarios and parameters settings.

$$\delta_{Q_{PCC}} = \frac{|\epsilon_{Q_{PCC}}|}{Q_{max}(PCC) - Q_{min}(PCC)} 100\% \quad (19)$$

A. Swedish 10kV rural distribution grid

This study case includes the same grid from the previous section with the same parameters, loading and disposition scenarios. The obtained results are given in Table III. Comparing the results obtained from analytical model in Table III with results from Tables I and II, the approximation error in all the studied cases is evaluated and given in Table IV.

Maximum value of the total relative approximation error $\delta_{Q_{PCC}}$ defined by (19) for all the loading scenarios and parameters settings is $\max(\delta_{Q_{PCC}}) = 1.91\%$. Comparing the results from Table IV, it can be seen that the error is the biggest in the case of exporting reactive power to the PCC ($Q_{max}(PCC)$) while importing active power from the PCC (loading 2). Furthermore, for all the cases where active powers flow predominantly in opposite direction from reactive

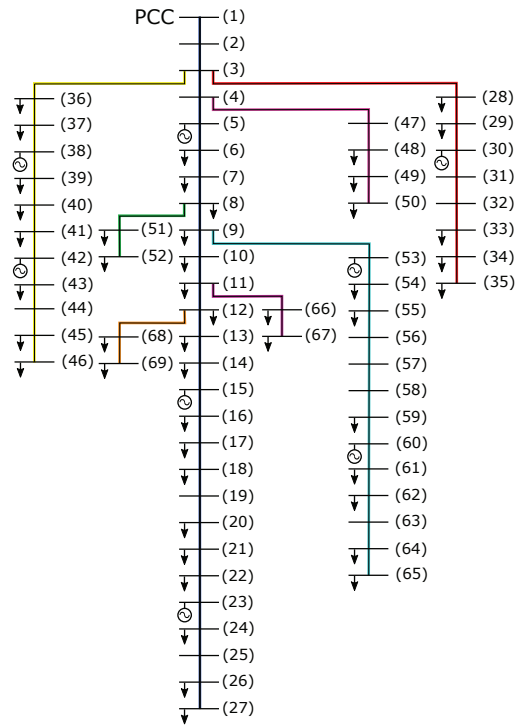


Fig. 9. IEEE 69 bus distribution grid with DG

powers in the grid, the approximation error is bigger. This fact was anticipated in derivation of analytical model from section III. With opposite flows of active and reactive power on the lines, angle differences between voltage phasors will increase consequently increasing the approximation error (5).

TABLE III
REACTIVE POWER PROVISION OF THE FIRST TEST SYSTEM CALCULATED USING DERIVED ANALYTICAL MODEL

	$Q_{PCC}[p.u.]$	overhead lines		cables	
		loading 1	loading 2	loading 1	loading 2
disp1	$Q_{min}(PCC)$	-7.4582	-1.6794	-10.3083	-0.2993
	$Q_{max}(PCC)$	1.5196	8.4699	1.7125	11.2728
disp2	$Q_{min}(PCC)$	-7.2432	-1.3773	-10.2563	0.5839
	$Q_{max}(PCC)$	1.9499	8.5640	2.7938	11.2639

TABLE IV
EVALUATED VALUES OF $\epsilon_{Q_{PCC}}$ FOR THE FIRST TEST SYSTEM

	$\epsilon_{Q_{PCC}}[p.u.]$	overhead lines		cables	
		loading 1	loading 2	loading 1	loading 2
disp1	$Q_{min}(PCC)$	-0.1104	-0.0714	-0.0363	-0.0139
	$Q_{max}(PCC)$	-0.0619	-0.1920	-0.0014	-0.0948
disp2	$Q_{min}(PCC)$	-0.0799	-0.0691	-0.0436	-0.0090
	$Q_{max}(PCC)$	-0.0007	-0.1230	-0.0052	-0.0563

B. IEEE 69 bus distribution grid

For the second test system, IEEE 69 bus 12.67kV distribution grid [33] is used. DFIG wind turbines with nominal power of 1.5 MW and reactive power limits defined by (2)

are integrated in the grid as shown on Fig. 9. The estimation of $Q_{max}(PCC)$ and $Q_{min}(PCC)$ using the OPF algorithm and (15) are done for four loading scenarios:

- 1) DG at 80% of maximum, consumption scaled 80%
- 2) DG at 80% of maximum, consumption scaled 120%
- 3) DG not producing (possible reactive support), consumption scaled 80%
- 4) DG not producing (possible reactive support), consumption scaled 120%

The obtained results are given in Table V and evaluated approximation error in Table VI. For this system, $\max(\delta_{Q_{PCC}})$ for the all loading scenarios is 0.79%.

TABLE V
REACTIVE POWER PROVISION OF THE SECOND TEST SYSTEM CALCULATED USING THE OPF ALGORITHM AND DERIVED ANALYTICAL MODEL

	$Q_{PCC}[p.u.]$	loading 1	loading 2	loading 3	loading 4
OPF	$Q_{min}(PCC)$	-0.9634	-1.0747	-1.2464	-1.1940
	$Q_{max}(PCC)$	0.3136	0.2064	0.9622	0.8521
(15)	$Q_{min}(PCC)$	-0.9460	-1.0575	-1.2415	-1.1843
	$Q_{max}(PCC)$	0.3251	0.1984	0.9701	0.8492

TABLE VI
EVALUATED VALUES OF $\epsilon_{Q_{PCC}}$ FOR THE SECOND TEST SYSTEM

$\epsilon_{Q_{PCC}}[p.u.]$	loading 1	loading 2	loading 3	loading 4
$Q_{min}(PCC)$	-0.0174	-0.0172	-0.0049	-0.0097
$Q_{max}(PCC)$	0.0115	0.0080	-0.0079	0.0029

C. Influence of parameter uncertainty on analytical estimation

Previous estimation of Q_{PCC} assumed perfect knowledge of all the grid parameters. Unfortunately, in practice this is mostly not the case. For example, resistance of lines might vary depending on operating conditions and outdoor temperature. To test the robustness of (15) on uncertainty of grid parameters, we assumed that resistance of the lines might vary $\pm 5\%$ from the original value. Applying this on IEEE 69 bus grid, results provided in Table VII are obtained. Associated error of estimation is given in Table VIII. For the case where R was overestimated $+5\%$, $\max(\delta_{Q_{PCC}}) = 1.82\%$. When R was underestimated, $\max(\delta_{Q_{PCC}}) = 1.77\%$. In both cases, the error increased for more than double but it still stayed less than 2% making (15) robust on uncertainty of the resistance of lines.

TABLE VII
ESTIMATION OF Q_{PCC} WHEN RESISTANCE OF LINES IS NOT PERFECTLY KNOWN

R	$Q_{PCC}[p.u.]$	loading 1	loading 2	loading 3	loading 4
$+5\%$	$Q_{min}(PCC)$	-0.9676	-1.0694	-1.2209	-1.1537
	$Q_{max}(PCC)$	0.3021	0.1847	0.9908	0.8795
-5%	$Q_{min}(PCC)$	-0.9244	-1.0456	-1.2621	-1.2149
	$Q_{max}(PCC)$	0.3481	0.2121	0.9493	0.8188

TABLE VIII
 $\epsilon_{Q_{PCC}}$ WHEN RESISTANCE OF LINES IS NOT PERFECTLY KNOWN

R	$\epsilon_{Q_{PCC}}[p.u.]$	loading 1	loading 2	loading 3	loading 4
$+5\%$	$Q_{min}(PCC)$	0.0042	-0.0053	-0.0255	-0.0403
	$Q_{max}(PCC)$	0.0115	0.0217	-0.0286	-0.0274
-5%	$Q_{min}(PCC)$	-0.0390	-0.0291	0.0157	0.0209
	$Q_{max}(PCC)$	0.0345	-0.0057	0.0129	0.0333

VI. FEED-FORWARD ESTIMATION

Maximum value of the total relative approximation error $\max(\delta_{Q_{PCC}})$ for all the scenarios analyzed in the previous section was less than 2%. Taking this into account, (15) can be used as a very good estimator of Q_{PCC} and can be included in the feed-forward control strategies as shown in Fig.10.

As inputs to the estimator block (EST), desired value of Q_{pcc} is given (Q_{pcc}^*) as well as non-controllable active and reactive power injections (P_{inj}^*, Q_{inj}^*). As outputs, controllable reactive power injections Q_{ff} can be calculated. Additionally, by adding the feedback loop to the control, $\epsilon_{Q_{PCC}}$ can be eliminated. Problem that arises when calculating Q_{ff} is that the U term and the loss term in (15) are dependent on P_{inj} and Q_{inj} . This means that (15) has to be complemented with estimation of U term and loss term as a function of P_{inj} , Q_{inj} and the grid parameters. This part exceeds the scope of this paper and should be included in a future research.

Since (15) is not explicitly putting any limits on reactive power injections, external limiter block has to be added to account for reactive power limits of the sources.

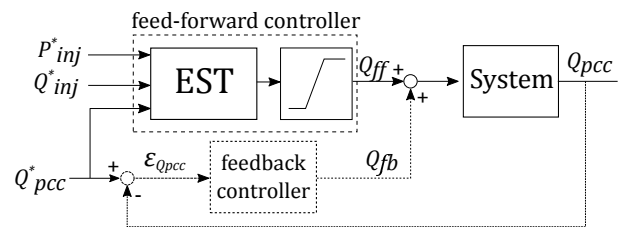


Fig. 10. Feed-forward control strategy

VII. DISCUSSION

Assessment of the grid's reactive power capability is usually done by running OPF algorithms for (1). If all the parameters of the system are known, these algorithms can calculate very accurately reactive power capability. Unfortunately, accuracy comes with the cost of computational time of these algorithms. When they are run over bigger time periods for multiple scenarios including contingency analysis, they require substantial computational power. Furthermore, qualitative conclusions about distribution grids' reactive power capability cannot be drawn from the OPF formulation (1).

The linearized analytical model proposed in this paper gives qualitative generalized results that apply to any radial distribution grid. Linearization comes at a cost of the approximation error presence. For the scenarios we tested, $\max(\delta_{Q_{PCC}}) < 2\%$. The future work should include how the approximation error behaves on the broader set of scenarios.

The analysis done in this paper was done assuming balanced, three-phase system. Distribution systems can often be unbalanced with multiphase lateral sections. For the future work, the model developed in this paper can be extended for unbalanced, multi-phase systems using similar methodology as in [34], [35]. It is mostly based on Fortescue transform and completing single-phase and two-phase lateral sections to three-phase sections by adding dummy lines and nodes.

VIII. CONCLUSIONS

Management of reactive power at the PCC between grids of different voltage levels is gaining significance with increasing penetration of DG in grids and deregulation. The grid codes are changing to enable greater flexibility in the grids. Reactive power markets are emerging. Estimation of reactive power capability of the grid and its enhancement will bring great benefits for distribution system operators in the future.

General conclusions about influence of different distribution grid parameters on its reactive power capability are drawn in this paper. Special attention has been put on a very common scenario: exchange of overhead lines with underground cables. It has been concluded that this particular change enhances reactive power capability of the grid. The conclusions have been drawn analytically from the derived linear model (Section III-B). Using the developed model, smart investment decisions can be made in the planning and development studies to improve capability of distribution grids to answer to the future challenges.

IX. ACKNOWLEDGMENT

The authors would like to thank Vattenfall, Sweden, for providing information concerning common network design.

REFERENCES

- [1] *EU Renewable Energy Directive 2009/28/EC*, European Union, 2009.
- [2] *The Paris Agreement 2015*, United Nations Framework Convention on Climate Change, 2005.
- [3] *Application Provisions (TILLÄMPNINGSGRÄNSBESTÄMMELSER)*, Vattenfall Eldistribution AB, 2017. [Online]. Available: <https://www.vattenfalldistribution.se/foretag/el-till-verksamheten/elnatpriset/>
- [4] *The Grid Code*, National Grid, 30 September 2016. [Online]. Available: <http://www2.nationalgrid.com/uk/industry-information/electricity-codes/grid-code/the-grid-code/>
- [5] *Technical guideline: Generating Plants Connected to the Medium-Voltage Network*, bdew, 2013. [Online]. Available: http://www.bdew.de/internet.nsf/id/DE_NetzCodes-und-Richtlinien
- [6] A. C. Rueda-Medina and A. Padilha-Feltrin, "Distributed generators as providers of reactive power support - a market approach," *IEEE Trans. Power Syst.*, vol. 28, no. 1, February 2013.
- [7] J. Zhong and K. Bhattacharya, "Reactive power market design and its impact on market power," in *IEEE PES General Meeting - Conversion and Delivery of Elect. Energy in the 21st Century*, July 2008.
- [8] Swissgrid, *Voltage Support Concept for the Swiss Transmission System*, swissgrid, 2011. [Online]. Available: <https://www.swissgrid.ch/en/home/customers/topics/ancillary-services/voltage-support.html>
- [9] *Commission Regulation (EU) 2016/1388 of 17 August 2016 establishing a Network Code on Demand Connection (Text with EEA relevance)*, European Commission. [Online]. Available: <http://eur-lex.europa.eu>
- [10] S. Auer, F. Steinke, W. Chunsen, A. Szabo, and R. Sollacher, "Can distribution grids significantly contribute to transmission grids' voltage management?" in *IEEE PES Innovative Smart Grid Technologies Conf. Europe (ISGT-Europe)*, 2016.
- [11] E. Diskin, P. Cuffe, and A. Keane, "Distribution system reactive power management under defined power transfer standards," in *IEEE PES General Meeting*, 2013.
- [12] T. Sowa, P. Goergens, A. Schnettler, R. Koberle, and M. Metzger, "Potential of the auw network area to provide reactive power to transmission network level," *Int. ETG Congress*, November 17-18 2015.
- [13] I. Talavera, S. Stepanescu, F. Bennewitz, J. Hanson, R. Huber, F. Oechsle, and H. Abele, "Vertical reactive power flexibility based on different reactive power characteristics for distributed energy resources," in *Int. ETG Congr.*, 2015.
- [14] P. Cuffe, P. Smith, and A. Keane, "Capability chart for distributed reactive power resources," *IEEE Trans. Power Syst.*, vol. 29, no. 1, pp. 15 - 22, January 2014.
- [15] D. S. Stock, A. Venzke, L. Löwer, K. Rohrig, and L. Hofmann, "Optimal reactive power management for transmission connected distribution grid with wind farms," in *IEEE Innovative Smart Grid Technologies - Asia (ISGT-Asia)*, 2016.
- [16] E. Sáiz-Marín, E. Lobato, I. Egido, and C. Gómez-Sánchez, "Voltage control assessment of wind energy harvesting networks," *IET Renewable Power Generation*, 2014.
- [17] D. S. Stock, A. Venzke, T. Hennig, and L. Hofmann, "Model predictive control for reactive power management in transmission connected distribution grids," in *IEEE PES Asia - Pacific Power and Energy Conf.*, 2016.
- [18] M. Frank, D. Konrad, L. Lothar, F. Luis, Mariano, H. Patrick, H. Lars, Henrik, and B. Martin, "Analysis of a reactive power exchange between distribution and transmission grids," in *Int. Workshop on Intelligent Energy Systems (IWIES)*, 2013.
- [19] Y. Christayakov, E. Kholodova, K. Natreba, A. Szabo, and M. Metzger, "Combined central and local control of reactive power in electrical grids with distributed generation," in *2nd IEEE ENERGYCON Conf. & Exhibition / Future Energy Grids and Systems Symp.*, 2012.
- [20] L. F. Ochoa, A. Keane, and G. P. Harrison, "Minimizing the reactive support for distributed generation: Enhanced passive operation and smart distribution networks," *IEEE Trans. Power Syst.*, vol. 26, no. 4, 2011.
- [21] S. Ali and J. Mutale, "Reactive power management at transmission/distribution interface," in *50th Int. Universities Power Engineering Conf. (UPEC)*, 1-4. September 2015.
- [22] P. Cuffe and A. Keane, "Voltage responsive distribution networks: Comparing autonomous and centralized solutions," *IEEE Trans. Power Syst.*, vol. 30, no. 5, September 2015.
- [23] E. Polymeneas and M. Benosman, "Finite time multi-agent coordination of distributed generation for grid reactive support," in *IEEE Innovative Smart Grid Technologies Conf. Asia (ISGT ASIA)*, 2014.
- [24] H. Wang, M. Kraiczky, S. Schmidt, F. Wirtz, C. Toebermann, B. Ernst, E. Kaempf, and M. Braun, "Reactive power management at the network interface of ehv- and hv level," *International ETG Congress*, 2017.
- [25] C. Kaloudas, L. F. Ochoa, B. Marshall, and S. Majithia, "Initial assessment of reactive power exchanges at uk grid supply points," in *CIREN Workshop*, Rome, 11-12 June 2014.
- [26] *Reactive Power Management at T - D Interface (ENTSO-E guidance document for national implementation for network codes on grid connection)*, ENTSO-E, 16 November 2016.
- [27] F. Hinz and D. Moest, "Techno-economic evaluation of 110 kv grid reactive power support for the transmission grid," *IEEE Trans. Power Syst.*, 2018.
- [28] T. Lund, P. Sørensen, and J. Eek, "Reactive power capability of a wind turbine with doubly fed induction generator," *Wind Energy*, vol. 10, pp. 379-394, April 2007.
- [29] G. Valverde and J. J. Orozco, "Reactive power limits in distributed generators from generic capability curves," *IEEE PES General Meeting*, July 27-31 2014.
- [30] M. Braun, "Reactive power supply by distributed generators," *IEEE PES General Meeting*, 2008.
- [31] R. D. Zimmerman, C. E. Murillo-Sanchez, and R. J. Thomas, "Matpower: Steady-state operations, planning and analysis tools for power systems research and education," *IEEE Trans. Power Syst.*, vol. 26, no. 1, pp. 12-19, Feb. 2011.
- [32] *Background Paper: Undergrounding of Electricity Lines in Europe*, Commission of European Communities, Brussels, 10 December 2003.
- [33] M. E. Baran and F. F. Wu, "Optimal capacitor placement on radial distribution systems," *IEEE Trans. Power Del.*, vol. 4, no. 1, January 1989.
- [34] I. Dzafic, S. Henselmeyer, and T. Donlagic, "Asymmetrical distribution power flow algorithm in fortescue coordinates," in *IEEE PES General Meeting*, 2012.
- [35] M. Abdel-Akher, K. M. Nor, and A.-H. Abdul-Rashid, "Development of unbalanced three-phase distribution power flow analysis using sequence and phase components," in *12th Int. Middle-East Power System Conf. (MEPCON)*, 2008.



Stefan Stanković (S'17) received the Dipl. Ing. and M.Sc. degrees in electrical engineering from University of Belgrade, Belgrade, Serbia, in 2014 and 2015, respectively. He is currently a PhD candidate at KTH Royal Institute of Technology, Sweden, Stockholm. His current research interests include integration of wind and solar power into power systems, reactive power support and voltage control of distribution and transmission grids, power systems control and stability.



Lennart Söder (M'91-SM'10) was born in Solna, Sweden, in 1956. He received the M.Sc. and Ph.D. degrees in electrical engineering from the KTH Royal Institute of Technology, Stockholm, Sweden, in 1982 and 1988, respectively. He is currently a Professor of Electric Power Systems with the KTH Royal Institute of Technology. His current research interests include power system operation and planning, integration of wind and solar power, hydropower system modelling, demand side management, distribution systems, power system reliability, power markets and regulation.